Impact of Nanosizing on Lithiated Rutile TiO_2

Wouter J. H. Borghols,[†] Marnix Wagemaker,*[,†] Ugo Lafont,[‡] Erik M. Kelder,[‡] and Fokko M. Mulder[†]

Fundamental Aspects of Materials and Energy, Department of Radiation, Radionuclides, and Reactors, Faculty of Applied Sciences, Delft University of Technology, Mekelweg 15, 2629JB Delft, The Netherlands, and Delft ChemTech, Faculty of Applied Sciences, Delft University of Technology, Julianalaan 136, 2628 BL Delft, The Netherlands

Received November 28, 2007. Revised Manuscript Received February 14, 2008

The structural behavior of both micro- and nanosized TiO_2 rutile upon Li-ion insertion was determined from neutron diffraction measurements. In the solid solution regime in microsized rutile, which extends up to $x \approx 0.07$ Li/Ti, the Li ions mainly reside at the tetrahedral position at low temperatures and at the octahedral position at higher temperatures. A rationale of this effect was found in the influence of lattice dynamics, illustrated by molecular dynamics simulations of the Li-ion diffusion in the rutile structure. Maximum (chemically) lithiated microrutile (~0.43 Li/Ti at room temperature) reveals the formation of a layered morphology, having a monoclinic symmetry (*P*2/*m*, space group 10) similar to the previously suggested layered hexagonal structure. In addition, abundant lattice strains were induced. Consistent with recent electrochemical studies, the nanosized rutile (needle-shaped ~11 nm × 11 nm × 43 nm) material was able to host a significantly higher amount of lithium, leading to a maximum composition of ~0.85 Li/Ti. In the nanomaterial, the solid solution domain extended up to $x = 0.15$ Li/Ti (i.e., further than in the micromaterial). This provides more evidence that reducing the crystallite size reduces the miscibility gap of two-phase reactions upon lithiation, especially when lattice mismatches lead to strains between the phases, such as recently was demonstrated for anatase TiO_2 (Wagemaker et al. *J. Am. Chem. Soc.* **2007**, *129*, 4323). Further lithiation of the nanomaterial up to Li/Ti = 0.53 resulted in a phase transition toward an intermediate phase, very similar to the original rutile phase but slightly deformed, reducing the symmetry to the monoclinic *P*2/*m* space group. Upon further Li-ion insertion, up to ~0.85 Li/Ti, this phase transformed toward another structure, again indexed by the monoclinic *P*2/*m* space group but now similar to the layered hexagonal $R\bar{3}m$ space group previously suggested to form in rutile TiO_2 upon lithiation. The presented structural results provide a consistent picture of Li-ion insertion in micro- and nanosized rutile TiO_2, relating structure, crystallite size, and electrochemical performance.

Introduction

In the past decade, the reduction of electrode crystallite particle sizes from conventional micrometers down to nanometers has emerged as a promising strategy to improve the current density, as is required in high powered applications such as hybrid and electrical cars.[1,2] The crystallite particle size reduction decreases the rate-limiting Li-ion transport distances through the solid-state electrode material, thereby increasing (dis-)charge rates. However, the properties and performance of nanosized materials also are altered due to intrinsic changes of the material properties and a larger impact of surface phenomena,[1,3–6] processes that are only recently beginning to be understood. Only very recently has the impact of crystallite size on phase morphology and stoichiometry been recognized, where the interface and surface energetics appear to be the driving forces.[7–9] Both in anatase Li_xTiO_2 and in Li_xFePO_4, the miscibility gap related to the first-order phase transition is decreased, leading to stable solid solution compositions for smaller crystallite particles. In anatase Li_xTiO_2, this is most likely the origin of the reduced diffusion coefficient found for nanosized

* Corresponding author. E-mail: m.wagemaker@tudelft.nl.
† Department of Radiation, Radionuclides, and Reactors.
‡ Delft ChemTech.

(1) Maier, J. Nanoionics: Ion transport and electrochemical storage in confined systems. *Nat. Mater.* **2005**, *4*, 805–815.
(2) Arico, A. S.; Bruce, P.; Scrosati, B.; Tarascon, J. M.; Van Schalkwijk, W. Nanostructured materials for advanced energy conversion and storage devices. *Nat. Mater.* **2005**, *4*, 366–377.
(3) Maier, J. Thermodynamic aspects and morphology of nano-structured ion conductors—Aspects of nano-ionics. Part I. *Solid State Ionics* **2002**, *154*, 291–301.
(4) Maier, J. Defect chemistry and ion transport in nanostructured materials—Part II. Aspects of nanoionics. *Solid State Ionics* **2003**, *157*, 327–334.
(5) Jamnik, J.; Maier, J. Nanocrystallinity effects in lithium battery materials—Aspects of nano-ionics. Part IV. *Phys. Chem. Chem. Phys.* **2003**, *5*, 5215–5220.
(6) Kavan, L.; Prochazka, J.; Spitler, T. M.; Kalbac, M.; Zukalova, M. T.; Drezen, T.; Gratzel, M. Li insertion into $Li_4Ti_5O_{12}$ (Spinel)—Charge capability versus particle size in thin-film electrodes. *J. Electrochem. Soc.* **2003**, *150*, 1000–1007.
(7) Wagemaker, M.; Borghols, W. J. H.; Mulder, F. M. Large impact of particle size on insertion reactions: A case of anatase Li_xTiO_2. *J. Am. Chem. Soc.* **2007**, *129*, 4323–4327.
(8) Meethong, N.; Huang, H. Y. S.; Speakman, S. A.; Carter, W. C.; Chiang, Y. M. Strain accommodation during phase transformations in olivine-based cathodes as a materials selection criterion for high-powered rechargeable batteries. *Adv. Funct. Mater.* **2007**, *17*, 1115–1123.
(9) Schimmel, H. G.; Huot, J.; Chapon, L. C.; Tichelaar, F. D.; Mulder, F. M. Hydrogen cycling of niobium and vanadium catalyzed nanostructured magnesium. *J. Am. Chem. Soc.* **2005**, *127*, 14348–14354.

10.1021/cm703376e CCC: $40.75
Published on Web 04/17/2008

crystallite particles,[10] although the overall effect of the reduced crystallite particle size leads to a significant improvement of the power density in the range of 0–0.5 Li/Ti.[11,12] Additionally, nanosizing also appears to increase the insertion capacity, leading to a theoretical maximum composition of ~1 Li/Ti in 7 nm anatase crystallite particles.[6]

An even more spectacular improvement was observed in rutile TiO_2 (*P*42/*mnm*, space group 136), which is the most common and stable form of TiO_2. Microsized rutile crystallite particles generally are reported to host only a negligible amount of Li ions,[13] although rutile does appear to be active at elevated temperatures.[14,15] The poor performance of rutile appears to be surprising in view of the high Li-ion diffusion coefficient reported, on the order of 10^{-6} cm^2 s^{-1}.[16,17] Most likely, the one-dimensional character of the diffusion[17,18] limits the Li-ion insertion over significant three-dimensional volumes, leading to the poor performance of microsized materials.[13] Recently, it was found that nanosizing strongly increases both the capacity (~0.85 Li/Ti) and the rate capability.[19–21] Additionally, the electrochemical cycling experiments on both micro- and nanosized rutile show a high degree of irreversibility.[15,19–21] After one cycle, the maximum obtainable load is decreased by a factor 2, to ~0.4 Li/Ti. A possible explanation is the large structural change that the initial rutile *P*42/*mnm* crystal undergoes upon lithium insertion. Electrochemical measurement of the potential in the galvanostatic mode indicates the possible formation of a new phase around $x = 0.4$ Li/Ti.[19] Both experiments[15,19] and calculations[22] suggest the formation of a hexagonal structure ($R\bar{3}m$, space group 166) in fully intercalated rutile, although a cubic rock salt structure ($Fm\bar{3}m$, space group 225) also has been reported.[21] Additionally, a low symmetry intermediate phase has been suggested,[18] but the existence as well as the exact structure are uncertain.

In an attempt to clarify the structural evolution of both micro- and nanosized rutile TiO_2 upon lithiation, this work presents a dedicated structural investigation using neutron diffraction. In this study, neutrons were preferred over X-rays because of their relative sensitivity to Li ions, which allows the detailed determination of Li-ion positions and fractions[23] necessary to obtain insight into the solid solution behavior. First, microsized rutile was investigated to determine the exact lithium position, maximum chemical intercalation fraction, phase transitions, and strains that occur. Second, phase transitions were studied that occurred during the different intercalation stages in the nanostructured material. In this work, we used crystallite particles or just crystallite to indicate a particle having a single crystalline phase, hence having no grain boundaries. When lithiation causes a second phase within the initially single phase crystalline particle, we refer to this as the domain size within the crystalline particle.

Materials and Methods

Sample Preparation and Chemical Lithiation. Two crystalline particle sizes were investigated: Needle-shaped nanocrystalline TiO_2 (rutile) and microsized crystalline particles were obtained from Sigma Aldrich. These materials were chemically lithiated with *n*-butyllithium (1.6 M, Sigma Aldrich).[24] This procedure is potentiostatic, and the over potential or driving force using *n*-butyllithium is 0.9 V versus Li^+/Li^0. To avoid lithium reacting with air and moisture, when possibly Li_2O, LiOH,[25] lithium-carbonates, and lithium-nitrates are formed, two precautions were taken. First, all powders were dried in a vacuum oven at ~373 K for at least 36 h, to ensure water-free pristine materials. Second, the intercalation procedure was performed in a glovebox under argon atmosphere having less than 2 ppm O_2 and moisture.

TEM, X-ray, and Neutron Diffraction. Structural characterization of the pristine TiO_2 crystalline structure was performed by means of X-Ray diffraction (Bruker D8 Avance using Cu Kα radiation), from which the crystalline purity was determined to be larger than 99%. Crystallite particle sizes were determined by the line-width broadening of the diffraction pattern in terms of the γ_2 parameter in GSAS. The instrumental contribution in γ_2 was subtracted, and the result was used to determine the particle size applying Scherrer's formula, with Scherrer's constant equal to unity. For the pristine materials, accurate values for the needle-shaped crystallites also were obtained with transmission electron microscopy (Philips CM30T operated at 300 kV), by statistically averaging ~100 observed crystallites. The results are presented in Table 1; the error margin represents the standard deviation in the crystallite particle size. Additionally, the atomic purity was verified with energy dispersive spectroscopy (EDS). Finally, the Li/Ti mol fraction of the lithium-inserted material was determined by wet chemical inductively coupled plasma (ICP) spectroscopy. The results from both ICP and TEM analyses are presented in Table 1.

(10) Wagemaker, M.; Borghols, W. J. H.; van Eck, E. R. H.; Kentgens, A. P. M.; Kearley, G. J.; Mulder, F. M. The influence of size on phase morphology and Li-ion mobility in nanosized lithiated anatase TiO_2. *Chem.—Eur. J.* **2007**, *13*, 2023–2028.
(11) Reiman, K. H.; Brace, K. M.; Gordon-Smith, T. J.; Nandhakumar, I.; Attard, G. S.; Owen, J. R. Lithium insertion into TiO_2 from aqueous solution—Facilitated by nanostructure. *Electrochem. Commun.* **2006**, *8*, 517–522.
(12) Kavan, L.; Fattakhova, D.; Krtil, P. Lithium insertion into mesoscopic and single-crystal TiO_2 (rutile) electrodes. *J. Electrochem. Soc.* **1999**, *146*, 1375–1379.
(13) Murphy, D. W.; Di Salvo, F. J.; Carides, J. N.; Waszczak, J. V. *Mater. Res. Bull.* **1978**, *13*, 1395–1402.
(14) Zachau-Christiansen, B.; West, K.; Jacobsen, T.; Atlung, S. Lithium insertion in different TiO_2 modifications. *Solid State Ionics* **1988**, *28*, 1176–1182.
(15) Macklin, W. J.; Neat, R. J. Performance of titanium dioxide-based cathodes in a lithium polymer electrolyte cell. *Solid State Ionics* **1992**, *53-6*, 694–700.
(16) Johnson, O. W. *Phys. Rev.* **1964**, *136*, A284—A290.
(17) Gligor, F.; de Leeuw, S. W. Lithium diffusion in rutile structured titania. *Solid State Ionics* **2006**, *177*, 2741–2746.
(18) Koudriachova, M. V.; Harrison, N. M.;. de Leeuw, S. W. Density-functional simulations of lithium intercalation in rutile. *Phys. Rev. B: Condens. Matter Mater. Phys.* **2002**, *65*, 235423–235435.
(19) Hu, Y. S.; Kienle, L.; Guo, Y. G.; Maier, J. High lithium electroactivity of nanometer-sized rutile TiO_2. *Adv. Mater.* **2006**, *18*, 1421–1426.
(20) Jiang, C.; Honma, I.; Kudo, T.; Zhou, H. Nanocrystalline rutile TiO_2 electrode for high-capacity and high-rate lithium storage. *Electrochem. Solid State Lett.* **2007**, *10*, 127–129.
(21) Baudrin, E.; Cassaignon, S.; Koelsch, M.; Jolivet, J.-P.; Dupont, L.; Tarascon, J.-M. Structural evolution during the reaction of Li with nano-sized rutile type TiO_2 at room temperature. *Electrochem. Commun.* **2007**, *9*, 337–342.
(22) Koudriachova, M. V.; Harrison, N. M.; de Leeuw, S. W. Effect of diffusion on lithium intercalation in titanium dioxide. *Phys. Rev. Lett.* **2001**, *86*, 1275–1278.
(23) Wagemaker, M.; Kearley, G. J.; van Well, A. A.; Mutka, H.; Mulder, F. M. Multiple Li positions inside oxygen octahedra in lithiated TiO_2 anatase. *J. Am. Chem. Soc.* **2003**, *125*, 840–848.
(24) Whittingham, M. S.; Dines, M. B. Normal butyllithium—Effective, general cathode screening agent. *J. Electrochem. Soc.* **1977**, *124*, 1387–1388.
(25) Södergren, S.; Siegbahn, H.; Rensmo, H.; Lindström, H.; Hagfeldt, A.; Lindquist, S.-E. Lithium intercalation in nanoporous anatase TiO_2 studied with XPS. *J. Phys. Chem. B* **1997**, *101*, 3087–3090.

Table 1. Crystallite Particle Size and Used Compositions of Materials[a]

crystallite particle size	fraction of Li/Ti
(11 ± 3) nm $\times$ (11 ± 3) nm $\times$ (43 ± 5) nm	0
	0.16 ± 0.02
	0.25 ± 0.03
	0.53 ± 0.02
	0.85 ± 0.02
microsized	0.1 ± 0.02
	0.43 ± 0.02

[a] Starting materials were obtained from Aldrich, the sizes were determined by TEM, and the Li/Ti ratio was determined from ICP spectroscopy.

Neutron diffraction measurements were performed at GEM, the high intensity general-purpose time-of-flight diffractometer at the ISIS pulsed neutron source (Rutherford Appleton Laboratory). GEM is equipped with more than 6000 detectors in seven banks covering angles between approximately 169° (backward scattering) and 7° (forward scattering). All samples were measured at room temperature, while the micromaterial was additionally measured at 10, 40, 70, and 110 K in airtight cylindrical vanadium sample cans with the initial idea that this would reduce the Li temperature factors. The resulting neutron diffraction spectra of several banks (91.3, 154.4, and 63.9°) were refined simultaneously using the Rietveld method as implemented in GSAS.[26] The *d*-spacing under consideration ranged from 0.3 to 4 Å. Besides the atomic and lattice parameters, the absorption and line-broadening parameters, the crystal phase fractions, and the background were fitted.

First-Principle Calculations. The nuclear density distribution with respect to time of the Li ions in the TiO_2 rutile structure, as well as the ground-state energies, was modeled using density functional theory (DFT) in the generalized gradient approximation (GGA) as implemented in the VASP plane wave pseudopotential code.[27] For the molecular dynamics, a 1 fs time step for a duration of 130 ps was used for a single Li atom in a $2 \times 2 \times 4$ (16 unit cells) primitive cell having 97 atoms, which was performed at several temperatures.

Results and Discussion of Microrutile

In Figure 1a, the neutron diffraction results for microsized TiO_2 rutile at intercalation fractions $x = 0.07$ and $x = 0.43$ mol are presented. To determine the exact position of lithium in the pristine rutile TiO_2 structure, a material with a small Li-ion intercalation fraction was prepared. The small Li-ion occupancies in the solid solution domain of charge–discharge curves indicate a solid solution regime of approximately $0 < x < 0.05$ Li/Ti at room temperature[19] and $0 < x < 0.1$ Li/Ti at $T = 120$ °C.[15] Such small Li-ion occupancies can be expected to cause only subtle changes in the diffraction pattern. Additionally, the expected large (anisotropic) diffusion coefficient of Li ions in the *c*-direction,[16–18] experimentally reported to be as large as $\sim 10^{-6}$ cm^2 s^{-1} at room temperature[16] and consistently predicted by calculations,[17] may interfere with the exact determination of the Li-ion position in the rutile lattice. For these reasons, a relatively long measurement (large signal-to-noise ratio) at 10 K was performed, which is presented in Figure 1a.

Although the Li-ion position in the rutile host has not been determined experimentally, it has been suggested to occupy the octahedral positions.[19] In contrast, calculations indicate that the tetrahedral position is energetically more favorable.[28,29] An experimental indication for the Li-ion position from neutron data in Figure 1a can be obtained by Fourier analysis of the difference between the observed structure factors and those calculated for the pristine rutile structure. The positions found, shown in Figure 1b, can subsequently be included in the Rietveld refinement, leading to more accurate Li-ion position(s) and occupation(s). In $Li_{0.1}TiO_2$ at $T = 10$ K, this leads to occupations 0.021 and 0.015 of the tetrahedral and octahedral sites, respectively, resulting in an overall composition of $Li_{0.07}TiO_2$. Since the tetrahedral occupation is larger, it may be concluded that this position is energetically favored, consistent with calculational studies.[28,29] The fact that both positions are occupied at 10 K indicates that the energy difference between the two sites is rather small. Assuming a Boltzmann law, the temperature dependence of these occupations can be used to estimate the energy difference between the tetrahedral and the octahedral sites.[23] For that reason, neutron diffraction patterns were measured at several temperatures, leading to the occupations shown in Figure 2a.

Raising the temperature toward room temperature (RT) reduces the tetrahedral occupation and increases the octahedral site occupation. However, a regular Boltzmann distribution should converge to equal occupation of both sites with increasing temperature. The fact that this does not happen, as is indicated in Figure 2a, indicates that another process influences the site occupation. To study the role of lattice dynamics, molecular dynamics simulations were performed. The model used consists of a single Li ion in a primitive cell built up of $2 \times 2 \times 4$ unit cells (32 Ti and 64 O atoms). Relaxation of the Li ion on the tetrahedral and octahedral position leads to a rather small difference in the ground-state energy of about 1.8 meV ($\sim$20 K) per atom, favoring tetrahedral over octahedral site occupation, consistent with previous studies.[18,22] Molecular dynamics simulations at 300 K up to 20 ps led to the Li-ion trajectory displayed in Figure 2b. The trajectory indicates that the Li ion mainly resides at the octahedral position (the squares in Figure 2b) before it hops toward the next octahedral site. Clearly, at 300 K, the simulation indicates predominantly an octahedral site occupation. Although this may not be expected based on the ground-state energies, it is consistent with Li-ion occupancies in Figure 2a experimentally determined by neutron diffraction, also indicating a predominant octahedral occupation at room temperature. Additionally, molecular dynamics simulations were performed at various temperatures where the Li ion was initially placed at the tetrahedral position. Below 30 K, the Li ion remained at the tetrahedral position; however, at higher temperatures, it moved immediately toward the octahedral position, consistent

(26) Larson, A. C. *GSAS* Los Alamos National Laboratory: Los Alamos, NM, 1994.
(27) Kresse, G.; Furthmuller, J. *Comput. Mater. Sci.* **1996**, *6*, 15–50.
(28) Stashans, A.; Lunell, S.; Bergstrom, R.; Hagfeldt, A.; Lindquist, S. E. Theoretical study of lithium intercalation in rutile and anatase. *Phys. Rev. B: Condens. Matter Mater. Phys.* **1996**, *53*, 159–170.
(29) Koudriachova, M. V.; Harrison, N. M.; de Leeuw, S. W. Open circuit voltage profile for Li-intercalation in rutile and anatase from first principles. *Solid State Ionics* **2002**, *152*, 189–194.

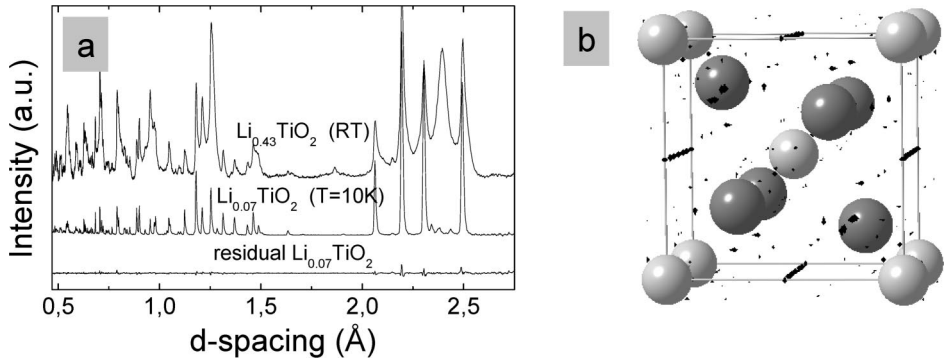

Figure 1. (a) Neutron diffraction patterns of microsized rutile Li_xTiO_2 for $x = 0.1$ Li/Ti ($T = 10$ K) and $x = 0.43$ Li/Ti (room temperature). The small reflections between 2.3 and 2.5 Å are due to traces of anatase in the rutile material, accounting for less than 2% of the material. (b) Fourier density difference map of the rutile $Li_{0.07}TiO_2$ neutron diffraction pattern (a) including oxygen atoms (dark gray) and Ti atoms (light gray). The four rows of black spots indicate the Li-ion occupation of the alternating octahedral−tetrahedral sites.

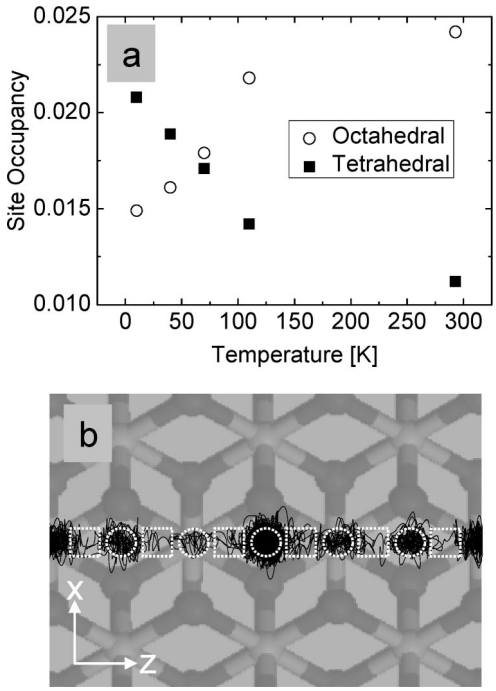

Figure 2. (a) Temperature dependent octahedral and tetrahedral site occupations from Rietveld refinement of rutile $Li_{0.07}TiO_2$. (b) Li-ion trajectory in a rutile TiO_2 supercell resulting from molecular dynamics simulations at $T = 300$ K for 130 ps. The amplitude of the diffusion in the x-direction was increased for clarity. The white dotted squares indicate tetrahedral sites, and the circles indicate octahedral sites.

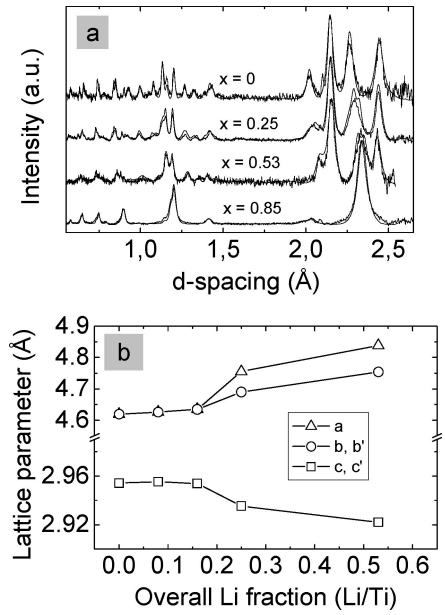

Figure 3. (a) Neutron diffraction patterns of nanosized Li_xTiO_2 rutile (black), including fit (gray) compositions of $x = 0$, 0.25, 0.53, and 0.85. (b) Changes of the unit cell lattice parameters in the different space groups (see text) as a function of lithium content.

with recent calculations.[17] Apparently, the lattice dynamics (phonons) above 20 K interact with the Li ions in such a way that octahedral site occupation becomes more likely. In general, one may say that the coupling of phonons with the Li ions enables the Li ions to lose kinetic energy—and thus stop—at the octahedral lattice position for some time. For the tetrahedral sites, this mechanism is apparently less effective. Therefore, we suggest that in rutile TiO_2, the Li ion effectively does not couple to the tetrahedral position at high temperatures, whereas it is able to lose energy to the lattice at the octahedral position, where it will reside shortly before hopping toward the next site. A detailed consideration of this mechanism falls outside the scope of this study; however, we are currently investigating this interesting mechanism in more detail. At this stage, we conclude that the observed occupancies in Figure 3a appear to be explained qualitatively by the molecular dynamics calculations.

It may be considered remarkable that molecular dynamics simulations are covering time scales long enough to observe the hopping of the Li ions in a crystalline phase in the first place. In general, this is limited to fast moving protons in metals because the Li-ion mobility in the Li-ion electrode compounds is too small to be simulated by DFT methods, and other approaches are required such as Monte Carlo methods.[22,30] However, in rutile TiO_2, the relatively large (anisotropic) diffusion coefficient, $\sim 10^{-6}$ cm^2 s^{-1},[16,17] enables picosecond calculations to be long enough to simulate a significant number of hops between the lattice voids of the rutile TiO_2 host structure.

The neutron diffraction fit results indicate a maximum Li/Ti composition of the micrometer-sized rutile material

(30) Van der Ven, A.; Ceder, G.; Asta, M.; Tepesch, P. D. First-principles theory of ionic diffusion with nondilute carriers. *Phys. Rev. B: Condens. Matter Mater. Phys.* **2001**, *64* (18), 184307(1)–184307(17).

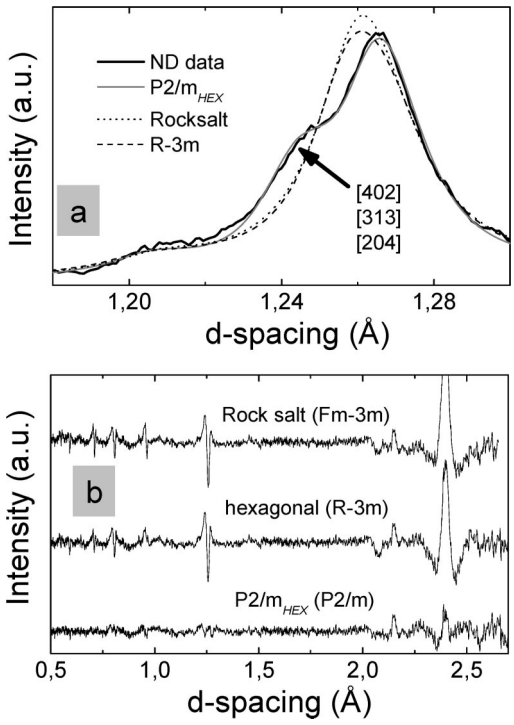

Figure 4. Molecular dynamics spectrum for $Li_{0.85}TiO_2$ as compared to three crystalline structures. (a) Results of all structures in their best fit result. (b) Residual of the best fits of each phase is plotted.

(chemically lithiated at RT with *n*-butyllithium) of $x = 0.43$ Li/Ti, which has been verified by ICP spectroscopy. The diffraction patterns in Figure 1a reveal a marked difference between the two compositions ($x = 0.1$ and $x = 0.43$). The appearance of the distinct peak around $d = \sim 2.4$ Å corresponds to the formation of a layered phase that can be indexed by the monoclinic space group 10, Laue symbol *P*2/*m*. Rietveld refinement indicates that approximately 44% of the material is transformed toward this layered phase. Because the atomic arrangement of this new phase closely resembles the hexagonal space group $R\bar{3}m$, which was suggested by X-ray diffraction[15,19] and predicted by calculations,[18,31] this new phase will be denoted with $P2/m_{(HEX)}$ for the remainder of this article. The structure is schematically shown in Figure 5, and the lattice parameters and atomic positions are listed in Table 2. The Li ions reside on the octahedral positions that form a two-dimensional layer, as illustrated in Figure 5. The lithium composition of this phase found by neutron diffraction, $x = \sim 0.8$ Li/Ti, is surprisingly large, in particular given the poor electrochemical activity of the micromaterial. Possibly, this is due to the long (in the order of days) exposure to an overload of *n*-butyllithium. The significant broadening in the diffraction pattern of this distorted hexagonal phase, clearly observed in Figure 1a, indicates that the newly formed phase hosts a significant amount of strain and/or has a reduced crystallite particle size as compared to the original rutile crystal phase. Assuming that all the broadening is due to crystallite size broadening, lithiation of the microsized TiO_2 rutile leads to ~20 nm crystallite particles having the original rutile structure and 8 nm crystallite particles having the $P2/m_{(HEX)}$ structure. Most likely, the large change in unit cell volume, ~13%, causes mechanical failure of the original micrometer-sized crystallites due to abundant strains, leading to the smaller crystallites. This breaking up of crystallites may explain the large irreversible capacity loss of microsized rutile observed in the cycling experiments.[19]

Table 2. Unit Cell Parameters and Atomic Positions of Rutile $Li_{0.07}TiO_2$ (10 K), $Li_{0.53}TiO_2$ $P2/m_{(RUT)}$ (RT), and $Li_{0.85}TiO_2$ $P2/m_{(HEX)}$ (RT)

Rutile Pristine Crystal	$a/b = 4.619$ Å, $c = 2.954$ Å, and $\alpha/\beta/\gamma = 90°$			
	*P*42/*mnm*			
$T = 293$ K	Ti	0	0	0
wRp = 0.028	O	0.3019	0.3019	0
Rp = 0.030	Li_I	0.5	0	0.5
	Li_{II}	0.5	0	0.25
Rutile Deformation	$a = 4.839$ Å, $b = 2.922$ Å, $c = 4.754$ Å, $\alpha = 90°$, $\beta = 88.91°$, and $\gamma = 90°$			
	$P2/m_{(RUT)}$, $x = 0.53$ Li/Ti			
$T = 293$ K	Ti_I	0	0	0
wRp = 0.0098	Ti_{II}	0.5	0.5	0.5
Rp = 0.0098	O_I	0.310	0	0.275
	O_{II}	0.807	0.5	0.185
	Li_I	0.5	0.5	0
	Li_{II}	0	0.5	0.5
Hexagonal Deformation	$a = 5.078$ Å, $b = 2.951$ Å, $c = 5.022$ Å, $\alpha = 90°$, $\beta = 71.7°$, and $\gamma = 90°$			
	$P2/m_{(HEX)}$, $x = 0.85$ Li/Ti			
$T = 293$ K	Ti_I	0	0.5	0.5
wRp = 0.0092	Ti_{II}	0.5	0	0.5
Rp = 0.0088	O_I	0.242	0	0.259
	O_{II}	0.270	0.5	0.747
	Li_I	0	0	0
	Li_{II}	0.5	0.5	0

Results and Discussion of Nanorutile

In Figure 3a, neutron diffraction patterns of nanosized rutile materials are presented that have different Li compositions. Fitting the composition of 0.16 Li/Ti (not shown in Figure 3a) revealed only the presence of the initial rutile phase (*P*42/*mnm*), having a Li occupancy of 0.15 Li/Ti. This suggests that the solubility of Li ions in the initial rutile crystallites is significantly larger in the nanomaterial (11 nm × 11 nm × 43 nm needles; see Materials and Methods for details) than in the microsized rutile material (where the solubility was found to be 0.07 Li/Ti). Figure 3b indicates that the Li insertion up to 0.15 Li/Ti is accompanied by a very small change in lattice parameters. Hu et al. suggested that up to $x = 0.15$ lithium is stored at the surface.[19] Our fit results indicate that a fraction of ~0.15 actually enters the rutile host structure, supported by the slight change in the lattice parameters. The current results therefore indicate that electrochemical charging should lead to solid solution behavior up to $x = 0.15$. Such solid solution behavior should result in a smoothly decreasing potential up to $x = 0.15$, consistent with what was observed.[19] Charging above $x = 0.15$ leads to a potential plateau in the charging curve reported,[19] indicative of two-phase behavior. This suggests that the surface storage capacity, if present, is small as compared to the capacity of the solid solution domain.

(31) Benco, L.; Barras, J.-L.; Daul, C. A.; Deiss, E. Theoretical study of the intercalation of Li in TiO_2 structures. *Inorg. Chem.* **1999**, *38*, 20–28.

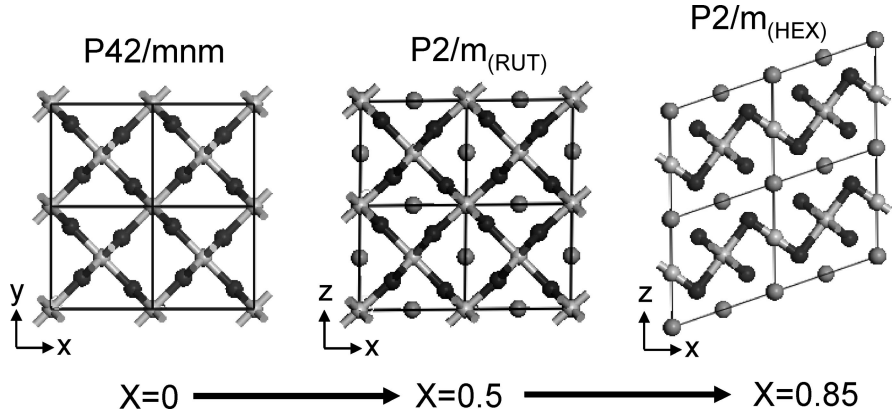

Figure 5. Structural evolution of nanoneedle rutile TiO_2 upon lithiation, where x indicates the composition (Li_xTiO_2).

Clearly, much more research is required to gain insight concerning these interesting phenomena related to the nanosizing of electrode materials. However, the present results are a direct indication that the solid solution domain is larger in the nanosized TiO_2 crystallite particles.

In the case of nanoscale anatase TiO_2[7] and also nanoscale $LiFePO_4$,[32,33] strains occurring between the different intercalated phases were indicated as a driving force for the alteration of the phase behavior in nanocrystallite particles. The crystallite particle size-induced enhancement of the solid solution domain appears to be the result of the relatively large energy penalty that is induced upon the formation of an interface within a small crystallite particle.[34] Instead of accommodating the interface, it becomes energetically favorable to extend the solid solution domain. The apparent absence of strains in the nanoneedles and the observed extended solid solution domain suggest that this mechanism is a more general phenomenon.

At insertion fraction $x = \sim 0.25$ of ~59% of the nanostructured rutile TiO_2 crystallite particles is converted from the initial tetragonal symmetry (*P*42/*mnm*) toward a new phase that could be indexed with the monoclinic space group 10 (*P*2/*m*). It is noteworthy that the absence of additional line broadening in the diffraction upon lithiation indicates that there is no phase coexistence (domains having a different crystal phase) within each crystallite particle; instead, 59% of all crystallite particles is converted completely to the monoclinic phase. At $x = 0.53$, the initial rutile symmetry is converted completely to this phase. In addition, roughly 5% of the material appears to be converted to the $P2/m_{(HEX)}$ phase found in the microsized rutile and later for nanosized rutile. The *P*2/*m* phase found at compositions of $x = 0.25$ and $x = 0.53$ should not be confused with that found in microsized rutile, which has the same symmetry but a different atomic arrangement (layered). In the case of nanorutile, the atomic positions and lattice parameters (see Table 2) lead to a structure that is very similar to the initial rutile structure. To emphasize the similarity with the pristine rutile structure, it will be referred to as $P2/m_{(RUT)}$. This similarity may not be immediately clear from Table 2 comparing lattice parameters and atomic positions but is evident from Figure 5, where only very subtle differences between the two structures are visible. The standard axis assignment is such that the rutile *P*42/*mnm* *b*-axis corresponds to the $P2/m_{(RUT)}$ *c*-axis. While the *a*-axis in both structures is directly comparable, the *b*- and *c*-axes are interchanged. For comparison, the $P2/m_{(RUT)}$ *b*-axis will be denoted as c', to emphasize the correlation with the rutile *c*-axis. Likewise, the $P2/m_{(RUT)}$ *c*-axis will be written as b' (see Figure 3b). The phase transition of the rutile phase toward the $P2/m_{(RUT)}$ phase involves a significant unit cell volume increase of ~6.3%. These two phases are most likely the origin of the plateau-like region observed from $x = 0.15$ up to $x = 0.4$.[19] Possibly, this newly observed phase also has an extended solid solution domain around the composition of $x = 0.5$, similar to the initial rutile structure, rationalizing the slope between $x = 0.4$ and $x = 0.5$ reported by Hu et al.[19]

Upon further lithiation, a smooth gradual step in the voltage profile was observed around $x = 0.5$ toward a second plateau-like region,[19] which may imply a second phase transition. The microrutile results suggest the formation of the $P2/m_{(HEX)}$ phase, which is very similar to the hexagonal $R\bar{3}m$ phase, the latter proposed by other authors both based on X-ray diffraction[15,19] and based on calculations.[18,31] In contrast, recent research reported the formation of the cubic rock salt structure in nanoscale rutile TiO_2.[21] Figure 4a,b presents the neutron diffraction data in addition to the best fits representing the three different proposed end structures of maximum lithiated nanostructured rutile. Fitting led to residuals of about 2.2% for both the rock salt ($Fm\bar{3}m$) and hexagonal ($R\bar{3}m$) structures, which can be considered to be quite accurate. However, an even more satisfying residual of less than 0.9% was found for the $P2/m_{(HEX)}$ phase, demonstrated in Figure 4a,b. A closer inspection of one of the main reflections in Figure 4a illustrates the better agreement of the $P2/m_{(HEX)}$ symmetry with the diffraction data, where the splitting of the single rock salt/$R\bar{3}m$ reflection is due to the lower symmetry of the monoclinic $P2/m_{(HEX)}$ space group.

(32) Yamada, A.; Koizumi, H.; Nishimura, S. I.; Sonoyama, N.; Kanno, R.; Yonemura, M.; Nakamura, T.; Kobayashi, Y. Room-temperature miscibility gap in Li_xFePO_4. *Nat. Mater.* **2006**, *5*, 357–360.
(33) Meethong, N.; Huang, H. Y. S.; Carter, W. C.; Chiang, Y. M. Size-dependent lithium miscibility gap in nanoscale $Li_{1-x}FePO_4$. *Electrochem. Solid State Lett.* **2007**, *10*, 134–138.
(34) Wagemaker, M.; Borghols, W. J. H.; Mulder, F. M. Large impact of size on insertion reactions: A case for Li_xTiO_2 anatase. *J. Am. Chem. Soc.* **2007**, *129*, 4323–4327.

Although the material was subjected to an overload of *n*-butyllithium, the composition did not exceed $Li_{0.85}TiO_2$, consistent with electrochemical lithiation.[19] Most likely, the theoretical capacity (1.0 Li/Ti) was not reached due to kinetic restrictions as a result of the high Li-ion occupancy. Similar results for nanostructured anatase TiO_2 suggest that reducing the crystallite particle size even further will lead to the theoretical capacity.[7] The similarity of $P2/m_{(HEX)}$ with the hexagonal $R\bar{3}m$ phase suggests that the Li_1TiO_2 composition will have the latter space group, as already was predicted by ab initio calculations.[18] The complete structural evolution of nanoneedles of rutile TiO_2 is schematically displayed in Figure 5. What remains is the question as to how the $P2/m_{(RUT)}$ phase (at composition $x = \sim 0.5$) transforms toward the $P2/m_{(HEX)}$ phase (at composition $x = 0.85$). The voltage profile during the first charge may indicate the presence of a plateau-like region, usually due to a two-phase transition.[19] The sloped character of this plateau-like region may indicate poor ionic diffusion, which may be expected for the $Li_{0.85}TiO_2$ ($P2/m_{(HEX)}$) phase. In contrast to the first phase transition in Figure 5, the second phase transition displays a radical rearrangement of the atoms in addition to a comparable 6% unit cell volume increase. Most likely, this structural transition explains the observed irreversible capacity loss during the first cycle, which does not take place if the material is cycled below compositions $x = 0.5$.[19] The first phase transition only leads to a ~6% volume increase, but the atomic arrangement does not change significantly (see Figure 5). This explains the good ability to cycle if the material is cycled below $x = 0.5$.[19] Above composition $x = 0.5$, Hu et al.[19] observed smaller crystalline particles together with amorphous regions with HRTEM, although the needle shape of the particles was preserved. Consistently, the diffraction indicates significant particle size broadening, which, if all is assumed to be due to crystallite particle size broadening, leads to an effective crystallite particle size of about 9 nm, whereas the pristine needles lead to an effective size of 12 nm.

Comparing the microrutile material with the nanomaterial, it may be considered a surprise that the microrutile material at composition $Li_{0.43}TiO_2$ can be indexed by $P2/m_{(HEX)}$ and not by $P2/m_{(RUT)}$, which is required to fit the nanomaterial with the similar composition of $Li_{0.53}TiO_2$. To understand this, we propose the following mechanism. Until the solid solution limit is reached, the one-dimensional diffusion takes care of rather homogeneous charging of the crystal, mostly starting from surfaces crossing the entrances of the one-dimensional channels. Upon further loading, however, the Li-rich $P2/m_{(HEX)}$ phase begins to be formed at the surface, which is most likely the reason for the poor electrochemical activity of the micromaterial.[13] The volume change of this transition is more than 12%, most likely leading to mechanical failure of the material, consistent with the observed broadening in the diffraction pattern of the micromaterial (Figure 1a).

Conclusion

Neutron diffraction of lithium intercalation in microsized TiO_2 rutile was compared to needle-shaped nanosized TiO_2 rutile powder. At low temperatures, Li ions mainly occupy the energetically favorable tetrahedral positions, whereas at room temperature, the octahedral positions appear to be favored. Molecular dynamics simulations indicate that lattice dynamics is responsible for this change in occupancy with temperature. Maximum lithiation of bulk rutile results in the formation of a layered structure, closely resembling the hexagonal phase $R\bar{3}m$, as suggested by previous studies. Li-ion insertion of nanosized needle-shaped rutile TiO_2 in the domain $0 < x < 0.5$ revealed an intermediate phase indexed by the monoclinic $P2/m$ space group, which is very similar to the initial tetragonal rutile $P42/mnm$ structure, hence referred to as $P2/m_{(RUT)}$. Further lithiation leads to a maximum composition *of* $x = 0.85$ Li/Ti, consistent with electrochemical charging, where the monoclinic $P2/m_{(RUT)}$ structure is transformed to a layered monoclinic structure also having the $P2/m$ space group. This layered structure closely resembles the hexagonal $R\bar{3}m$ structure and is therefore referred to as $P2/m_{(HEX)}$, which may be expected to form at the maximum theoretical composition Li_1TiO_2. The phase transition from $P2/m_{(RUT)}$ toward $P2/m_{(HEX)}$ may explain the large irreversible capacity loss found electrochemically, whereas the smaller structural changes between pristine rutile and $P2/m_{(RUT)}$ may explain the good reversibility at lower Li contents. Interestingly, the present results indicate that reducing the crystallite particle size promotes the solid solution behavior, similar to what was recently found in lithiated nanosized anatase TiO_2,[7] in nanosized Li_xFePO_4,[34] and also in H insertion in MgH_2,[9] suggesting this to be a more general phenomenon.

Acknowledgment. This work is a contribution from the Delft Institute for Sustainable Energy (DISE). Financial support from The Netherlands Organization for Scientific Research (NWO) is acknowledged for both beamtime at ISIS and the CW-VENI grant of M.W. We thank Winfried Kockelmann and Laurent Chapon for assistance with the neutron diffraction measurements at GEM (ISIS). We thank the Alistore network for providing access to TEM measurements.

CM703376E